Catalysis Today 390-391 (2022) 335–342

Contents lists available at ScienceDirect

Catalysis Today

journal homepage: www.elsevier.com/locate/cattod

Platinum nanoparticles supported on zeolite MWW nanosheets prepared via homogeneous solution route

Katarzyna Kałahurska [a], Wojciech Pajerski [a], Andrzej Kotarba [a], Martin Kubů [b], Yuyan Zhang [b], Michal Mazur [b], Jan Přech [b], Gabriela Jajko [a], Wacław Makowski [a], Wieslaw J. Roth [a], Barbara Gil [a,*,1]

[a] Faculty of Chemistry, Jagiellonian University in Kraków, Gronostajowa 2, 30-387 Kraków, Poland
[b] Department of Physical and Macromolecular Chemistry, Faculty of Science, Charles University, Hlavova 8, 12840 Prague 2, Czech Republic

ARTICLE INFO

Keywords:
Pt nanoparticles
MWW zeolites
Exfoliation
3-nitrotoluene hydrogenation

ABSTRACT

This article demonstrates preparation of metal functionalized zeolite catalysts via a new homogeneous solution pathway enabled by the recently reported exfoliation of zeolite MWW into solution of unilamellar nanosheets. The preparation is carried out by mixing solutions of exfoliated MWW monolayers and Pt nanoparticles with initial size of ca 3 nm and isolation of such hybrid catalysts by freeze-drying. Optionally, the MWW layer solutions were purified by dialysis prior to mixing with the metal solution, which turned out to be beneficial for quality and textural characteristics. However, catalytic performance in the model reaction – 3-nitrotoluene hydrogenation, was mostly determined by the Pt level, i.e. at least 0.3%, and less affected by the apparent quality of the final zeolite support. The catalysts revealed agglomeration of the Pt nanoparticles from roughly 3 nm to between 5 and 10 nm.

1. Introduction

Crystalline microporous solids with uniform, nanometer size pores, represented by zeolites, have exceptional value and usefulness in heterogeneous catalysis with many large-scale applications in the chemical and petroleum industries [1,2]. As they combine suitable high activity and selectivity with durability, lack of toxicity and ease of production, they are one of the leading catalysts for green chemistry. Zeolites are used by themselves and as supports or active components with other active moieties like metals. The main impediment to the broader application of zeolites has been related to their relatively small pore sizes constrained within rigid immutable frameworks. One of the attempted solutions was creation of additional, usually non-uniform, secondary porosity within zeolite structures by soft- or hard-templating, partial framework elimination, and other methods [3–8]. A more controlled approach was presented by the discovery that zeolites can form not only rigid 3D rigid frameworks but also layered 2D structures [9–13] that were amenable to structure modification, especially expansion [14–17]. One among many new capabilities enabled by layered zeolites has been the preparation of noble metal nanoparticles with controlled dispersion and accessibility via 2D-to-3D zeolite transformation for shape-selective catalysis [18]. In general, 2D zeolites could be manipulated spatially and intercalated with guest molecules and particles larger than their framework pores sizes. The intercalation and layer manipulation processes involve solid-liquid interactions and are also subject to limitations due to charge, layer affinity, reactant solubility and apparently crystal intergrowths. These constrains and the potential to design new catalysts have been further expanded by the complete exfoliation into monolayers in solution demonstrated with zeolite MCM-56 with the MWW topology [19]. The exfoliation is carried out as a soft chemical process by reacting MCM-56 with tetrabutylammonium hydroxide (TBAOH) in water that produces zeolite monolayers dispersed in a liquid as effectively homogeneous solutions [19]. They allow combination with any additional component ‘at will’, subject to compatibility and mutual affinity, which can be also considered adjustable. This work explores the combination of dispersed zeolite layers with Pt nanoparticles as alternatives to the aforementioned 2D-to-3D transformation. One of the differences/advantages worth pointing to is elimination of the swelling, which requires large excess of surfactant as generally complicated and, if possible, avoidable step.

* Correspondence to: Jagiellonian University, Faculty of Chemistry, Gronostajowa 2, 30-387 Kraków, Poland.
E-mail address: barbara.k.gil@uj.edu.pl (B. Gil).
[1] 0000-0003-4096-0762.

https://doi.org/10.1016/j.cattod.2021.09.026
Received 28 June 2021; Received in revised form 4 September 2021; Accepted 23 September 2021
Available online 25 September 2021

Metal nanoparticles (NPs) are of great interest for catalysis and have been extensively studied [20–27]. Nanoclusters and subnanoclusters of platinum (< 1 nm) have shown superb catalytic properties, which result from the small particle size and thus, high dispersion of active components [28]. Decreasing size of metal nanoparticle usually results in higher and faster conversion of substrates, but as shown by Guo et al. [29], there is typically an optimum size for best performance. Additionally, there is a tendency for irreversible aggregation of nanoparticle clusters resulting in a considerable recent effort to prevent that [30,31]. Dispersing metal particles on solid supports remains the most effective way to alleviate metal aggregation. Much attention was already given to promising solid supports, such as graphite [32], polymers [33], metal oxides [34] and zeolites [35–38].

The model reaction used in this study is hydrogenation of 3-nitrotoluene. Transformation of nitroarenes to anilines is of great practical importance owing to the usage of resulting anilines for dyestuffs and pharmaceuticals [39,40]. Furthermore, catalytic hydrogenation using high-pressure hydrogen with supported Pt as a catalyst is the preferred process [41]. Various support materials prepared by different methods exhibit substantial differences in catalytic activity. Zeolite based Pt-MWW materials can compete with different systems by showing fast conversion and high selectivity to m-toluidine as the only product [18].

The solutions of zeolite monolayers that are currently available with the MWW topology but are possible with other frameworks, can be combined with prepared metal nanoparticles in a second solution and eventually isolated as intimately mixed solids/catalysts. Such processes have many parameters that need investigation for optimized performance and benefits, e.g. synthesis and cost, that are very likely to depend on a particular catalytic reaction. Herein, we demonstrate high catalytic activity of the catalysts prepared from exfoliated monolayers and Pt nanoparticles and examine the effects of some basic properties and treatments during preparation.

2. Materials and methods

All reagents used in the experiments were purchased from Sigma-Aldrich except trimethylacetonitrile (Avantor Performance Materials Poland), trisodium citrate dihydrate (TSC, Avantor Performance Materials Poland), ammonium nitrate (NH_4NO_3, Avantor Performance Materials Poland), sodium aluminate (40–45% Na_2O, 50–56% Al_2O_3, Riedel-de-Haën).

2.1. Synthesis of MCM-56

MCM-56 was prepared by the published procedure [19,42]. The synthesis mixture comprised the following reagents: silica (nanopowder with particle size 10–20 nm), 50% NaOH solution, sodium aluminate, 98% hexamethyleneimine (HMI) and deionized water combined with the molar ratios: 1 SiO_2: 0.04 Al_2O_3: 0.093 Na_2O: 0.3 HMI: 16 H_2O. The hydrothermal synthesis was carried out in a sealed Teflon-lined autoclave with rotation, initially by aging for 12 h at room temperature, and then with heating at 145 °C for 38 h. The solid product was isolated by filtration, washed with deionized water and dried at room temperature. Its quality was verified by powder X-ray diffraction (XRD) and textural parameters.

2.2. Exfoliation and purification of MWW monolayer solutions

The published two-step procedure was followed [19]. 0.5 g of MCM-56 was stirred for 1.5 h with 27 g of 11% tetrabutylammonium hydroxide (TBAOH) solution and centrifuged for 20 min at 10,000 rpm in a 50 ml falcon tube (Kartell, non-sterile). The supernatant was decanted and discarded. 40 ml of water was added to the wet sediment, stirred for 1.5 h and centrifuged like before. The obtained translucent supernatant solution containing unilamellar MWW nanosheets [19], was carefully decanted and used, as-is or after dialysis, for combination with Pt-nanoparticle solutions described below. Typical pH was 12.

2.3. Dialysis of the MWW nanosheet solutions

The dialysis was carried out as an optional purification/pH reduction step. Supernatant solutions with MWW layers were poured into a dialysis tubing cellulose membrane with the cutoff of 14,000 Daltons (Sigma-Aldrich) and immersed in excess deionized water. The external solvent was stirred and changed repeatedly, until the desired pH was obtained.

2.4. Synthesis of the platinum nanoparticles

Citrate-capped platinum nanoparticles were synthesized with the protocol described elsewhere [43]. In a typical procedure, 2 ml of H_2PtCl_6 (16.0 mM) and 2 ml of TSC (40.0 mM) were added to 76 ml of deionized water and stirred for 30 min at room temperature. Next, 200 µl of $NaBH_4$ (50.0 mM) was added dropwise and the reaction mixture was stirred vigorously for 1 h at ambient temperature. The typical particle size was 1.5–3.5 nm.

2.5. Preparation of MWW zeolite-Pt samples

Solutions with platinum nanoparticles were added dropwise to 40 ml of the solutions of MWW nanosheets with stirring. The mixture was stirred for additional 20 min and lyophilized. The following solution ratios were used to obtain desired Pt contents: 1:1.175 (0.8% Pt w/w), 1:0.44 (0.3% Pt w/w), and 1:0.30 (0.2% Pt w/w).

2.6. Freeze-drying

The solutions of Pt nanoparticles and MWW monolayers (50–90 ml) were frozen for 30 min in a shell bath freezer to − 42 °C, with integrated rotate system and then attached to the lyophilizer (Labconco®) and maintained under vacuum (0.1 mbar) for overnight, affording low density powder.

2.7. Sample preparation for catalysis

The obtained Pt-MWW zeolite samples were calcined at 540 °C for 6 h to remove the template and other organic residue, and ion exchanged into the NH_4^+ form, by stirring with 1 M solution of NH_4NO_3 for 1 h at room temperature (20 ml of NH_4NO_3 per 0.5 g zeolite). The exchange was carried out three times, then samples were filtered, washed with deionized water and dried at room temperature.

2.8. Catalyst characterization

Fourier-Transform Infrared Spectroscopy (FT-IR) was used to determine the concentration of Brønsted (BAS), Lewis (LAS) and external Brønsted (BAS_{ext}) sites. Pyridine (kinetic diameter 0.54 nm [44]) adsorption allowed to determine BAS and LAS concentration, using intensity of the 1545 cm^{-1} band of protonated pyridine, and the 1450 cm^{-1} band of coordinatively bonded pyridine with respective absorption coefficients: ε(BAS) = 0.044 cm^2/µmol, ε(LAS) = 0.165 cm^2/µmol [45]. Trimethylacetonitrile (pivalonitrile, kinetic diameter 0.62 nm [44]) interacts only with Brønsted acid sites at the external surfaces and pore mouths. External Brønsted acid sites (BAS_{ext}) concentration was estimated by integration of the 3620 cm^{-1} maximum, characteristic of Si-OH-Al group, i.e. BAS [46] measured before and after trimethylacetonitrile adsorption. Self-supporting pellets of mass between 15 and 20 mg were prepared from zeolite powders, and transferred to a home-made FT-IR cell, allowing activation and adsorption inside FT-IR spectrometer. Samples were calcined at 490 °C for 1 h under vacuum (~ 10^{-5} mbar). Before the adsorption of probe molecules the system was cooled to the proper adsorption temperature: 170 °C for pyridine,

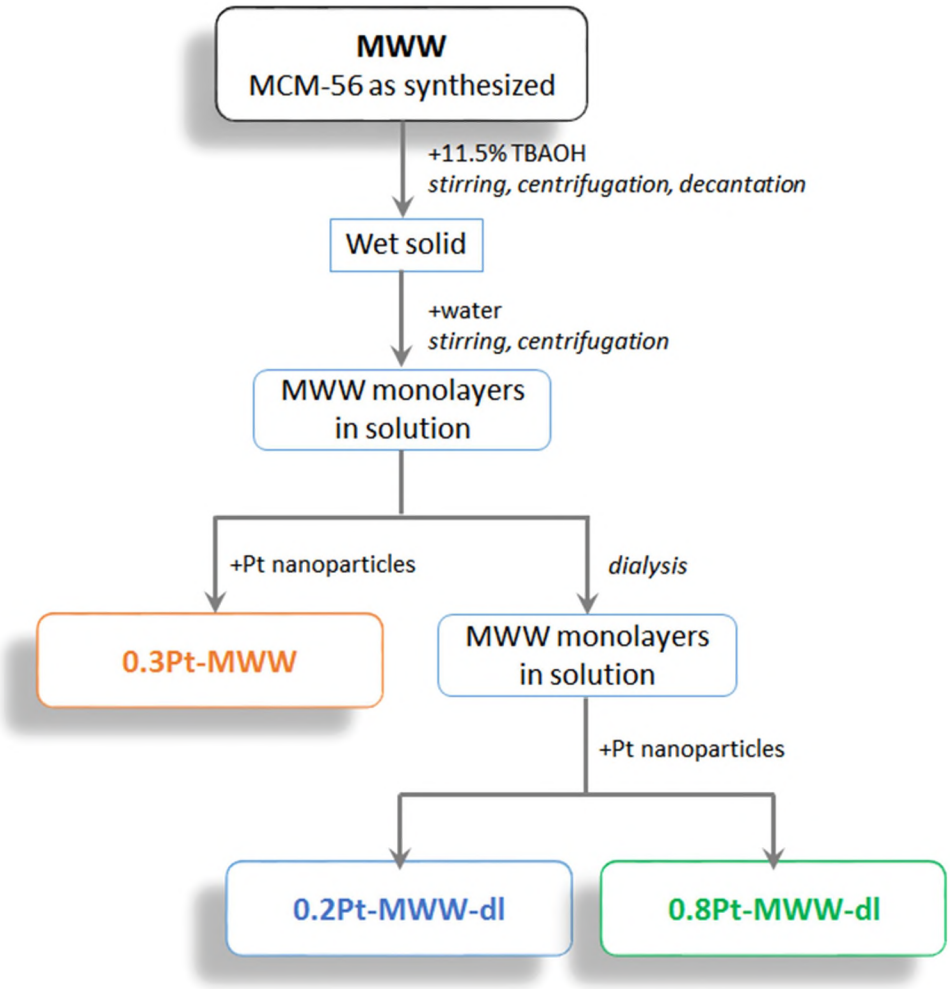

Scheme 1. Preparation steps leading to Pt-MWW materials.

ambient temperature for pivalonitrile. After adsorption of the vapors (at ca. 20 mbar equilibrium pressure) the gas phase together with weakly adsorbed species were evacuated at the adsorption temperature for 20 min. FT-IR measurements were carried out using the Bruker Tensor 27 spectrometer equipped with an MCT detector having the spectral resolution of 2 cm^{-1}.

The solid products were characterized by X-ray diffraction (XRD) using Rigaku MiniFlex diffractometer in refection mode, CuKα radiation ($\lambda = 0.154$ nm) in the ranges $2\theta = 3–35°$. The XRD patterns were usually collected with steps of 0.02°.

Adsorption/desorption isotherms of nitrogen at − 196 °C were determined using static volumetric Autosorb IQ apparatus (Quantachrome Instruments). All samples were activated under vacuum for 1 h at 80 °C, 1 h at 120 °C and 8 h at 350 °C (2 °C/min). Specific surface area values were determined using the BET method, based on the recommendation concerning characterization of microporous materials [47]. The t-plot method was used to determine the external surface area and micropore volume values.

TEM measurements were performed using an FEI S/TEM Titan instrument operating at an accelerating voltage of 300 kV. TEM visualization was also carried out using JEOL NeoARM 200 F operating at 200 kV. STEM images were collected using annular dark field detector. Powder samples were deposited on the EMR Holey Carbon support film on copper 300 square mesh. Microscope was aligned by the standard method using sample covered with gold nanoparticles. The measurements were carried out to assess the morphology and size distribution of the synthesized platinum nanoparticles. TEM images were analyzed using the Java open-source ImageJ 1.51k software [48].

2.9. Catalytic testing

The model catalytic reaction was performed in PID 4 Parallel Stirred Tanks Ppcstr19003. Before the reaction, the Pt-MWW catalysts were reduced in a tube oven with 150 ml/min H_2/N_2 (v:v = 1:1) at 500 °C for 5 h (4 °C/min). Catalytic reactors with 50 ml volume were loaded with ~ 7.5 mmol of 3-nitrotoluene (Sigma Aldrich, 99%), ~ 50 mg catalysts (Pt-MWW or Pt/Al_2O_3 – Sigma Aldrich, 1% loading), ~ 2.5 mmol n-dodecane (Sigma Aldrich, 98%, internal standard), and 30 ml n-hexane (VWR Chemicals, 100%). After reaching 100 °C, the autoclave was pressurized with 6 bar H_2 and stirring was fixed at 800 rpm. Samples of the reaction mixture were withdrawn after 0, 15 min, 30 min, 1 h, 2 h, 4 h, and 6 h of the reaction. The samples were centrifuged to remove the catalyst and analyzed by gas chromatography using a gas chromatograph Agilent 7890B GC equipped with HP-5 column (length 30 m, diameter 0.32 mm, and film thickness 0.25 μm).

The conversion of 3-nitrotoluene (Conv.) and was calculated according to Eq. (1):

$$\mathrm{Conv}(\%) = \frac{N_{3n\ feed} - N_{3n\ pr}}{N_{3n\ feed}} \cdot 100\% \quad (1)$$

where $N_{3n\ feed}$ is the amount of 3-nitrotoluene (moles) in the feed; $N_{3n\ pr}$ is the amount of 3-nitrotoluene (moles) in the products mixture. All N values used in Eq. (1) were calculated based on the internal standard calibration method, using n-dodecane as an internal standard and

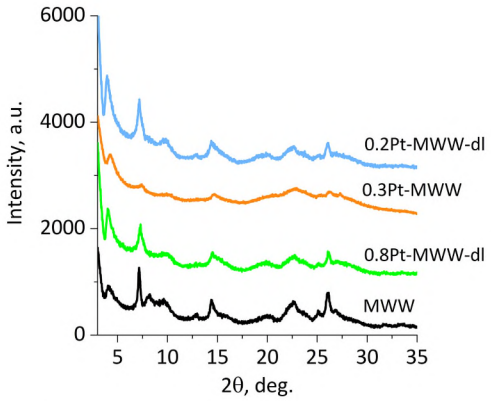

Fig. 1. XRD patterns of MCM-56 with platinum nanoparticles and their parent (MWW).

commercially available 3-nitrotoluene. For identification of the product m-toluidine (Sigma Aldrich, 99%) was used.

3. Results and discussion

The primary goal of this work has been the preparation and validation of a new type of zeolite-metal nanoparticle catalysts that have been enabled by the availability of exfoliated zeolite monolayer solutions. The liquid dispersions of zeolite monolayers and metal nanoparticles in solutions are prepared separately and combined into homogeneous solutions from which intimate solid mixtures can be isolated. Freeze-drying was the chosen method of isolation as it ensured full recovery of all components. Before the reported exfoliated zeolite layers in solution [19] become available the only possible synthetic pathways were based on solid-liquid treatments [44,49], which are constrained in many ways, especially by size and charge as obstacles to mutual component penetration and intimate mixing. These impediments are in principle absent and the synthesis is readily implemented in the systems presented herein, because they are based on forming homogeneous liquid solutions. One of the important parameters that may be critical for activity and cost, is the relative amount the metal, so it was investigated as the primary variable, between nominal 0.2–0.8% Pt metal. The preparations proved to be straightforward and produced the desired outcome of Pt-nanoparticles with representative sizes below 10 nm well dispersed within the zeolite matrix. This was confirmed by TEM and more detailed physical characterization. Most notably, the obtained catalysts showed potential for high activity, dependent on Pt level, in a model reaction – 3-nitrotoluene hydrogenation, with performances comparable to a commercial catalyst. The preparation and differences between the produced catalysts are shown in Scheme 1. The adopted sample designation includes %Pt and optional -dl at the end (as dialysis if applied, e.g. 0.2Pt-MWW-dl).

In all preparations the original framework was preserved but there was some variation in basic zeolite characteristics: XRD, textural properties and acidity, which turned out to be less crucial for high catalytic activity.

Powder X-ray diffraction patterns of the Pt-nanoparticle-MWW layers (Pt-MWW) after calcination, shown in Fig. 1, contain the fingerprint reflections at ca. 7.1°, 14.2°, 25° and 26°2θ (CuKα radiation; d-spacing: 1.25, 0.625, 0.356, 0.342 nm) confirming the MWW structure [50]. The original MCM-56 samples show the characteristic broad band between 8° and 10°2θ, assigned to disorganized MWW layers but with a slight dip, interpreted as partial ordering due to calcination [51]. In the Pt-MWW this band is not well defined because there is an additional distinct broad maximum arising near 10°2θ. The latter was already reported in our previous publication concerning MWW layers isolated after exfoliation [52] but its origin and assignment are obscure. One of the possibilities may be that it is related to the 003 reflection. The

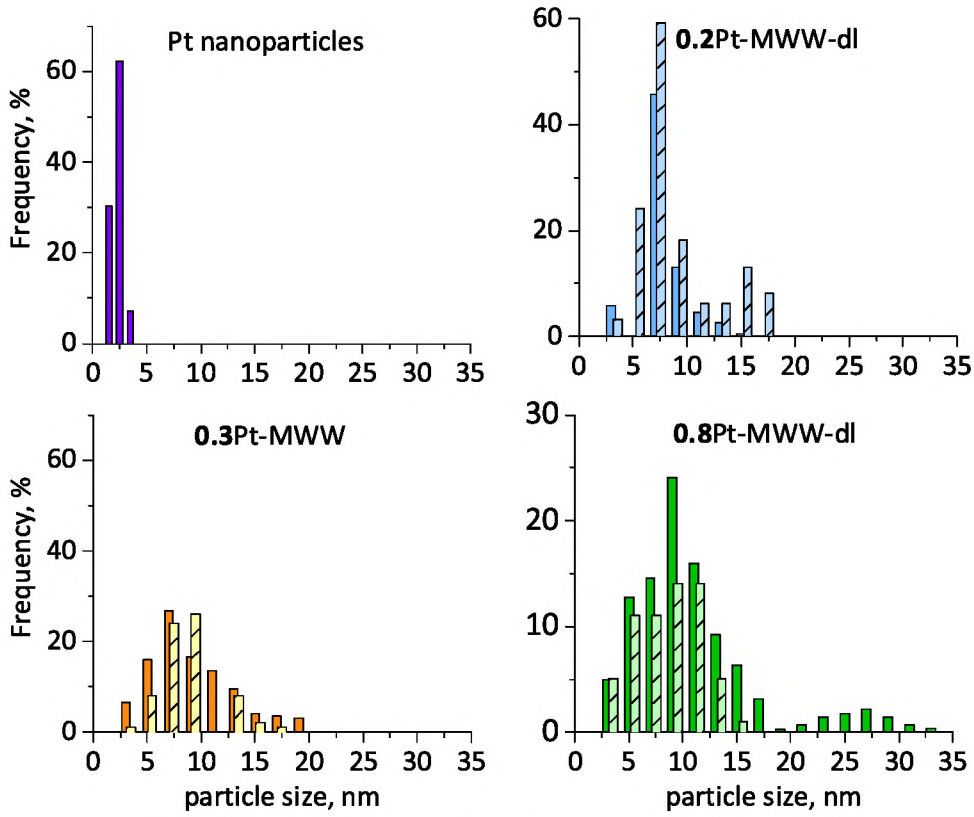

Fig. 2. Particle size distribution (PSD) in the original platinum nanoparticles solution, in calcined and ammonium exchanged Pt-MWW materials (darker colors) and after reduction with H_2 (striped).

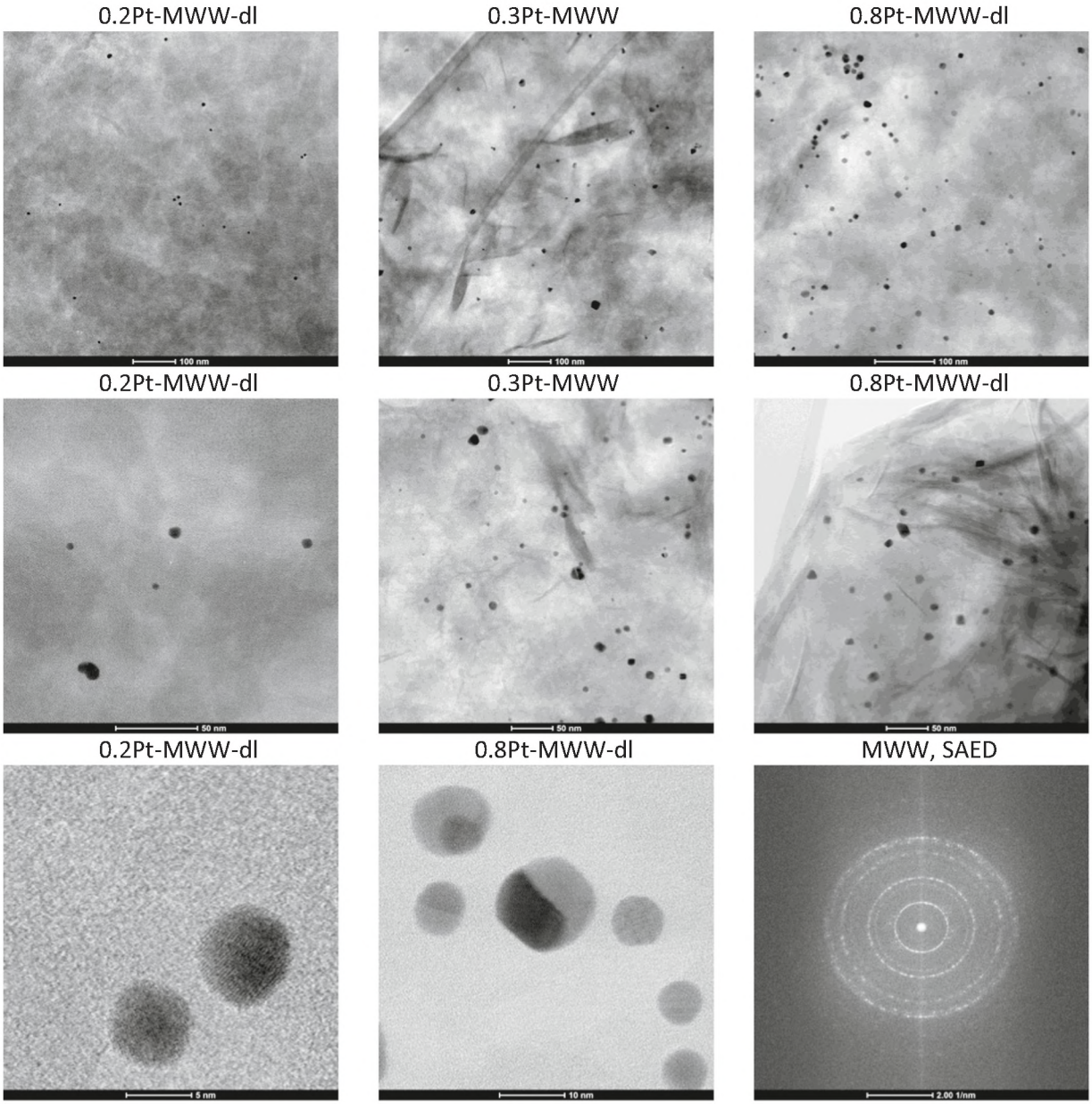

Fig. 3. Selected TEM images for the Pt-MWW materials (rows 1 and 2), close-up view of selected samples of the Pt nanoparticles (bottom left) and SAED of the zeolite (bottom right).

Table 1
Acid sites concentration based on the sorption of pyridine (total Brønsted and Lewis acid sites, BAS and LAS) and pivalonitrile (external Brønsted acid sites, BAS_{ext}) determined by FT-IR spectroscopy, and textural properties calculated from nitrogen adsorption isotherms (specific surface area BET, micropore volume, and external surface area).

Sample	Surface area, m^2/g		Pore volume, cm^3/g	Acid sites concentration, μmol/g		
	S_{BET}	S_{ext}	V_{micro}	BAS	LAS	BAS_{ext}
MWW	504	201	0.104	1028	142	376
0.2Pt-MWW-dl	507	291	0.092	826	158	196
0.3Pt-MWW	255	329	0	554	98	254
0.8Pt-MWW-dl	431	269	0.070	831	141	253

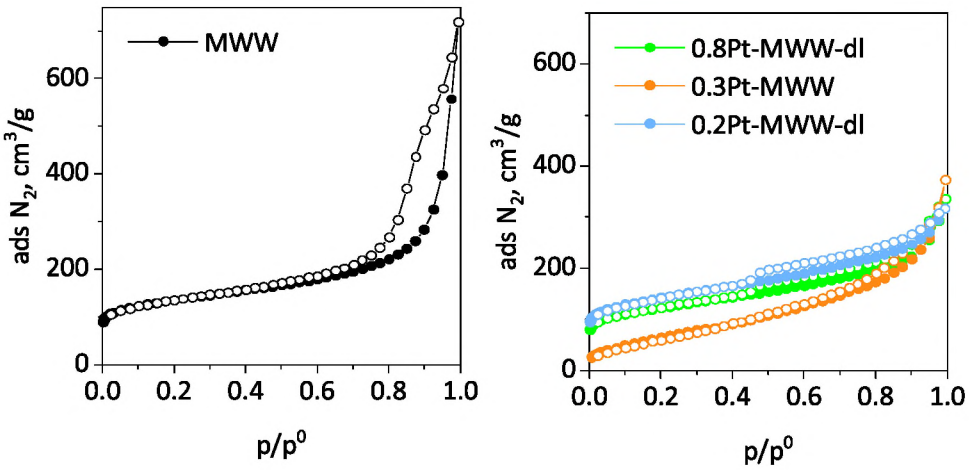

Fig. 4. N_2 adsorption isotherms for parent MWW and Pt-MWW samples.

Pt-MWW materials show amplified low angle reflections at 3.8°2θ, which are not the 001 reflections but due to non-Bragg diffraction caused by thin crystal dimension along the z axis [53,54]. The observed intensity amplification may indicate that due to Pt-nanoparticles the layers reveal more unilamellar character that when they condense without intervening particles. The sample obtained without dialysis of the solution with MWW layers has visibly lower crystallinity, which is also reflected in lowered textural parameters. Evidently, dialysis is conducive to higher crystallinity and porosity, but these parameters are not crucial for the eventual overall catalytic performance.

Particle size distributions of the Pt nanoparticles are shown in Fig. 2. The original nanoparticles in solution are not larger than 3.5–4 nm. The dominant size fractions are 2.5 nm (62%) and 1.5 nm (30%). The size of Pt nanoparticles in the zeolite matrix after calcination is increased to between 5 and 10 nm for the most abundant fraction and the size distribution is broadened. There is evident agglomeration and the resultant particles have continuous crystalline structure. Larger amount of Pt, namely 0.8%, leads to bigger particles overall, so the smaller amounts, like 0.3% seem optimal (for cost reasons too) (Fig. 3).

The combined results of textural properties calculated from nitrogen adsorption isotherm (specific surface area BET, micropore volume, and external surface area) and concentration of Brønsted active sites are summarized in Table 1.

For the Pt-MWW samples the final textural properties are greatly influenced by pre-purification of the MWW nanosheet solutions by dialysis: the dialyzed ones, 0.2% and 0.8% Pt, showed significant micropore volume and BET surface areas, comparable to the source MCM-56 materials. In contrast, the undialyzed MWW solution resulted in the end in depressed textural properties and also lowered apparent crystallinity (0.3%Pt). The dialyzed Pt-MWW samples showed ca. 30% higher external surface area and ca. 50% higher Brønsted acidity with respect to the sample not subjected to dialysis. The observed differences, especially the apparent lower quality of the undialyzed sample were not critical for catalytic performance.

There is a visible qualitative change in the isotherms (Fig. 4) between the original MCM-56 and the Pt-MWW products. The former show large vertical hysteresis above $p/p^0 > 0.8$, attributable to relatively large interparticle voids – it is type H2b due to pore blocking/percolation in a wide range of pore openings [47]. The dialyzed Pt-MWW samples showed very similar adsorption isotherms with a H3/H4 horizontal hysteresis loops, often exhibited by non-rigid agglomerates, platy-shaped microporous materials (H3) or aggregates of zeolite crystals (H4) [47]. The isotherm observed for the undialyzed sample is shifted down, which indicates significantly lower microporosity, and exhibits slightly larger slope indicating larger external surface. The fact that the BET surface is lower than the external surface areas is surprising

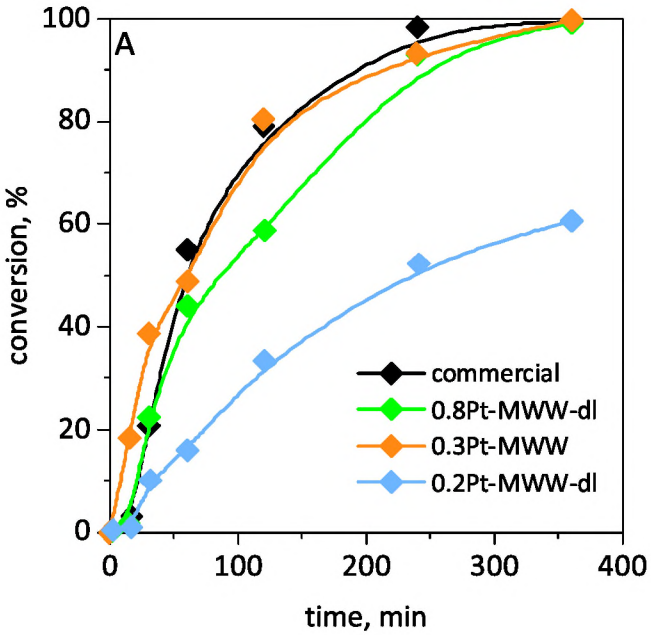

Fig. 5. Catalytic test results of 3-nitrotoluene hydrogenation.

but not erroneous, because both values were calculated using different formalism based on different geometrical models, therefore they have limited physical meaning and are not commensurate. 0.3Pt-MWW sample shows discrepancy between the data from nitrogen adsorption measurements (in which this material appears as non-porous) and acidity and catalysis data (which indicate considerable content of accessible acid sites, typical for zeolitic frameworks). A possible explanation of this effect is blocking the micropores by Pt nanoparticles, effective at liquid nitrogen temperature and ineffective at higher temperatures (due to thermal expansion and framework dynamics).

External acidity of all Pt-doped samples was significantly lower with respect to the source materials. BAS concentration decreased by ca. 25% (ca. 200 μmol/g) for the dialyzed samples and this loss is mainly due to the decrease of the BAS_{ext} concentration, which diminished from 376 to 200–250 μmol/g even as the external surface area increased. This can be accounted for, since Pt nanoparticles are located in the interparticle region, and their presence does not influence the internal (intralayer) acidity. At the same time pyridine was able to react with all BAS present, since the intensity of the Si-OH-Al maximum after pyridine adsorption disappeared (spectra not shown), which indicated that interior of the

layers was not blocked by the deposited nanoparticles. Much higher decrease of BAS concentration (ca. 50%) together with negligible micropore volume shown by the undialyzed sample highlights the importance of additional purification but is hard to explain in detail. On the other hand, such purification, e.g. by dialysis, was not crucial for hydrogenation activity as already emphasized above. This indicates the importance of colloid purification, in our case made by dialysis, in processes in which acidity is equally important as activity provided by nanoparticles.

As the final and most consequential evaluation, the obtained Pt-MWW materials were tested in a model catalytic reaction of 3-nitrotoluene hydrogenation (Fig. 5). The top conversion was comparable to a commercial catalyst, validating the general synthetic methodology and approach to producing competitive catalyst. The three studied samples showed differences in activity (with 100% selectivity to 3-aminotoluene), which are difficult to correlate with determined physical characteristics and acidity but point to a rationale that there is a minimum level for Pt, 0.3%, to achieve maximum conversion and above that the performance levels off. The 0.2% Pt catalyst is visibly less active than those 0.3% Pt and up. As already emphasized the nominal quality based on XRD, textural properties and acidity are less critical. In the same vain, dialysis affords better quality materials based on these properties but does not affect catalytic performance at this level. Possible sintering of Pt nanoparticles during activation of the catalysts in hydrogen at high temperature was ruled out on the basis of particle size distribution by TEM imaging. The overall distribution of the particle sizes was not changed considerably as shown in Fig. 2 (corresponding images of the H_2-treated catalysts are presented in Fig. S1, Supplementary material).

4. Conclusions

Zeolite MWW monolayers, 2.5 nm thick, exfoliated into solution were combined with solution of Pt nanoparticles, and isolated as intimately mixed solid catalysts. This represents an unprecedented approach to preparation of bifunctional catalysts, which to date was carried out exclusively via heterogeneous solid-liquid interactions. 3 different levels of platinum incorporation were targeted: 0.2%, 0.3% and 0.8% w/w with optional purification of the MWW solutions by dialysis after exfoliation. The obtained catalysts were tested in a model nitrotoluene hydrogenation and those with Pt content above 0.2% showed activity comparable to a benchmark commercial catalyst. Physical characterization showed that the applied dialysis was beneficial for XRD quality and textural properties but did not matter much for catalytic activity, which depended mostly on the amount of Pt, specifically to be at sufficiently high level (0.3% in this case). The final catalysts showed moderate increase in size of the Pt nanoparticles from ca. 3 nm to between 5 and 10 nm for the most represented size fraction. The demonstrated approach can be extended to both other exfoliated layered zeolites as they become available and other nanoparticles relevant for catalysis. The synthesis itself has many variables for optimization that may vary depending on a particular process.

CRediT authorship contribution statement

Katarzyna Kałahurska: Investigation, Conceptualization, Writing – original draft. **Wojciech Pajerski:** Investigation. **Andrzej Kotarba:** Investigation. **Martin Kubů:** Investigation. **Yuyan Zhang:** Investigation. **Michal Mazur:** Investigation. **Jan Přech:** Investigation. **Gabriela Jajko:** Investigation. **Wacław Makowski:** Writing – review & editing. **Wieslaw J. Roth:** Conceptualization, Funding acquisition, Writing – original draft, Writing – review & editing. **Barbara Gil:** Investigation, Writing – original draft, Writing – review & editing.

Declaration of Competing Interest

The authors declare that they have no known competing financial interests or personal relationships that could have appeared to influence the work reported in this paper.

Acknowledgments

This work was financed with the funds from the National Science Centre, Poland, Grant no. 2020/37/B/ST5/01258 (WJR and BG). KK has been partly supported by the National Centre for Research and Development, Poland, EU Project POWR.03.02.00-00-I004/16. MK and YZ acknowledge the support of the Czech Science Foundation, Czech Republic, to the project EXPRO (19-27551X).

Glassware for graphical abstract designed by macrovector/brgfx/Freepik.

Appendix A. Supplementary material

Supplementary data associated with this article can be found in the online version at doi:10.1016/j.cattod.2021.09.026.

References

[1] A.F. Masters, T. Maschmeyer, Zeolites – from curiosity to cornerstone, Microporous Mesoporous Mater. 142 (2011) 423–438.
[2] I. Fechete, Y. Wang, J.C. Vedrine, The past, present and future of heterogeneous catalysis, Catal. Today 189 (2012) 2–27.
[3] D. Verboekend, S. Mitchell, J. Perez-Ramirez, Hierarchical zeolites overcome all obstacles: next stop industrial implementation, Chimia 67 (2013) 327–332.
[4] D. Verboekend, J. Perez-Ramirez, Design of hierarchical zeolite catalysts by desilication, Catal. Sci. Technol. 1 (2011) 879–890.
[5] D. Verboekend, R. Caicedo-Realpe, A. Bonilla, M. Santiago, J. Perez-Ramirez, Properties and functions of hierarchical ferrierite zeolites obtained by sequential post-synthesis treatments, Chem. Mater. 22 (2010) 4679–4689.
[6] J. Perez-Ramirez, D. Verboekend, A. Bonilla, S. Abello, Zeolite catalysts with tunable hierarchy factor by pore-growth moderators, Adv. Funct. Mater. 19 (2009) 3972–3979.
[7] J. Perez-Ramirez, C.H. Christensen, K. Egeblad, C.H. Christensen, J.C. Groen, Hierarchical zeolites: enhanced utilisation of microporous crystals in catalysis by advances in materials design, Chem. Soc. Rev. 37 (2008) 2530–2542.
[8] J.C. Groen, J.A. Moulijn, J. Perez-Ramirez, Decoupling mesoporosity formation and acidity modification in ZSM-5 zeolites by sequential desilication-dealumination, Microporous Mesoporous Mater. 87 (2005) 153–161.
[9] L. Xu, P. Wu, Diversity of layered zeolites: from synthesis to structural modifications, New J. Chem. 40 (2016) 3968–3981.
[10] W.J. Roth, B. Gil, B. Marszalek, Comprehensive system integrating 3D and 2D zeolite structures with recent new types of layered geometries, Catal. Today 227 (2014) 9–14.
[11] U. Diaz, A. Corma, Layered zeolitic materials: an approach to designing versatile functional solids, Dalton Trans. 43 (2014) 10292–10316.
[12] W.J. Roth, D.L. Dorset, Expanded view of zeolite structures and their variability based on layered nature of 3-D frameworks, Microporous Mesoporous Mater. 142 (2011) 32–36.
[13] M. Choi, K. Na, J. Kim, Y. Sakamoto, O. Terasaki, R. Ryoo, Stable single-unit-cell nanosheets of zeolite MFI as active and long-lived catalysts, Nature 461 (2009) 246–249.
[14] L. Wei, K.C. Song, W. Wu, S. Holdren, G.H. Zhu, E. Shulman, W.J. Shang, H. Y. Chen, M.R. Zachariah, D.X. Liu, Vapor-phase strategy to pillaring of two-dimensional zeolite, J. Am. Chem. Soc. 141 (2019) 8712–8716.
[15] W.J. Roth, B. Gil, A. Mayoral, J. Grzybek, A. Korzeniowska, M. Kubu, W. Makowski, J. Cejka, Z. Olejniczak, M. Mazur, Pillaring of layered zeolite precursors with ferrierite topology leading to unusual molecular sieves on the micro/mesoporous border, Dalton Trans. 47 (2018) 3029–3037.
[16] H. Gies, U. Muller, B. Yilmaz, T. Tatsumi, B. Xie, F.S. Xiao, X.H. Bao, W.P. Zhang, D. De Vos, Interlayer expansion of the layered zeolite precursor RUB-39: a universal method to synthesize functionalized microporous silicates, Chem. Mater. 23 (2011) 2545–2554.
[17] W.J. Roth, C.T. Kresge, J.C. Vartuli, M.E. Leonowicz, A.S. Fung, S.B. McCullen, MCM-36: the first pillared molecular sieve with zeolite properties, Catal. Microporous Mater. 94 (1995) 301–308.
[18] Y. Zhang, K. Fulajtarova, M. Kubu, M. Mazur, M. Shamzhy, M. Hronec, J. Cejka, Controlling dispersion and accessibility of Pd nanoparticles via 2D-to-3D zeolite transformation for shape-selective catalysis: Pd@MWW case, Mater. Today Nano 8 (2019), 100056.
[19] W.J. Roth, T. Sasaki, K. Wolski, Y. Song, D.M. Tang, Y. Ebina, R.Z. Ma, J. Grzybek, K. Kalahurska, B. Gil, M. Mazur, S. Zapotoczny, J. Cejka, Liquid dispersions of zeolite monolayers with high catalytic activity prepared by soft-chemical exfoliation, Sci. Adv. 6 (2020) 8163.
[20] K. Ament, D.R. Wagner, T. Gotsch, T. Kikuchi, J. Krohnert, A. Trunschke, T. Lunkenbein, T. Sasaki, J. Breu, Enhancing the catalytic activity of palladium nanoparticles via sandwich-like confinement by thin titanate nanosheets, Acs Catal. 11 (2021) 2754–2762.

[21] D. Astruc, Introduction: nanoparticles in catalysis, Chem. Rev. 120 (2020) 461–463.
[22] J.Y. Cheon, S.J. Kim, W.H. Park, Facile interpretation of catalytic reaction between organic dye pollutants and silver nanoparticles with different shapes, J. Nanomater. 2019 (2019) 1–8.
[23] E.K. Dann, E.K. Gibson, R.H. Blackmore, C.R.A. Catlow, P. Collier, A. Chutia, T. E. Erden, C. Hardacre, A. Kroner, M. Nachtegaal, A. Raj, S.M. Rogers, S.F.R. Taylor, P. Thompson, G.F. Tierney, C.D. Zeinalipour-Yazdi, A. Goguet, P.P. Wells, Structural selectivity of supported Pd nanoparticles for catalytic NH_3 oxidation resolved using combined operando spectroscopy, Nat. Catal. 2 (2019) 157–163.
[24] R. Grisel, K.J. Weststrate, A. Gluhoi, B.E. Nieuwenhuys, Catalysis by gold nanoparticles, Gold Bull. 35 (2002) 39–45.
[25] S.C. Kim, W.G. Shim, M.S. Lee, S.C. Jung, Y.K. Park, Preparation of platinum nanoparticle and its catalytic activity for toluene oxidation, J. Nanosci. Nanotechnol. 11 (2011) 7347–7352.
[26] R.M. Rioux, H. Song, M. Grass, S. Habas, K. Niesz, J.D. Hoefelmeyer, P. Yang, G. A. Somorjai, Monodisperse platinum nanoparticles of well-defined shape: synthesise characterization, catalytic properties and future prospects, Top. Catal. 39 (2006) 167–174.
[27] E. Shahbazali, V. Hessel, T. Noel, Q. Wang, Metallic nanoparticles made in flow and their catalytic applications in organic synthesis, Nanotechnol. Rev. 3 (2014) 65–86.
[28] T. Imaoka, H. Kitazawa, W.J. Chun, K. Yamamoto, Finding the most catalytically active platinum clusters with low atomicity, Angew. Chem. Int. Ed. 54 (2015) 9809–9815.
[29] K. Guo, H. Li, Z. Yu, Size-dependent catalytic activity of monodispersed nickel nanoparticles for the hydrolytic dehydrogenation of ammonia borane, ACS Appl. Mater. Interfaces 10 (2018) 517–525.
[30] S.L. Allen, J.N. Sharma, F.P. Zamborini, Aggregation-dependent oxidation of metal nanoparticles, J. Am. Chem. Soc. 139 (2017) 12895–12898.
[31] B. Gilbert, R.K. Ono, K.A. Ching, C.S. Kim, The effects of nanoparticle aggregation processes on aggregate structure and metal uptake, J. Colloid Interface Sci. 339 (2009) 285–295.
[32] B. Bowden, M. Davies, P.R. Davies, S. Guan, D.J. Morgan, V. Roberts, D. Wotton, The deposition of metal nanoparticles on carbon surfaces: the role of specific functional groups, Faraday Discuss. 208 (2018) 455–470.
[33] G. Romanazzi, A.M. Fiore, M. Mali, A. Rizzuti, C. Leonelli, A. Nacci, P. Mastrorilli, M.M. Dell'Anna, Polymer supported Nickel nanoparticles as recyclable catalyst for the reduction of nitroarenes to anilines in aqueous medium, Mol. Catal. 446 (2018) 31–38.
[34] C.H. Mejia, J.E.S. van Der Hoeven, P.E. de Jongh, K.P. de Jong, Cobalt-nickel nanoparticles supported on reducible oxides as Fischer-Tropsch catalysts, ACS Catal. 10 (2020) 7343–7354.
[35] L. Liu, A. Corma, Confining isolated atoms and clusters in crystalline porous materials for catalysis, Nat. Rev. Mater. 6 (2021) 244–263.
[36] M. Shamzhy, M. Opanasenko, P. Concepción, A. Martínez, New trends in tailoring active sites in zeolite-based catalysts, Chem. Soc. Rev. 48 (2019) 1095–1149.
[37] S.-M. Wu, X.-Y. Yang, C. Janiak, Confinement effects in zeolite-confined noble metals, Angew. Chem. Int. Ed. 58 (2019) 12340–12354.
[38] S. Goel, Z. Wu, S.I. Zones, E. Iglesia, Synthesis and catalytic properties of metal clusters encapsulated within small-pore (SOD, GIS, ANA) zeolites, J. Am. Chem. Soc. 134 (2012) 17688–17695.
[39] I. Sorribes, A. Corma, Nanolayered cobalt–molybdenum sulphides (Co–Mo–S) catalyse borrowing hydrogen C–S bond formation reactions of thiols or H_2S with alcohols,, Chem. Sci. 10 (2019) 3130–3142.
[40] J. Song, Z.-F. Huang, L. Pan, K. Li, X. Zhang, L. Wang, J.-J. Zou, Review on selective hydrogenation of nitroarene by catalytic, photocatalytic and electrocatalytic reactions, Appl. Catal. B: Environ. 227 (2018) 386–408.
[41] A.-M. Alexander, J.S.J. Hargreaves, Alternative catalytic materials: carbides, nitrides, phosphides and amorphous boron alloys, Chem. Soc. Rev. 39 (2010) 4388–4401.
[42] W.J. Roth, P. Chlubna, M. Kubu, D. Vitvarova, Swelling of MCM-56 and MCM-22P with a new medium – surfactant-tetramethylammonium hydroxide mixtures, Catal. Today 204 (2013) 8–14.
[43] G.W. Wu, S.B. He, H.P. Peng, H.H. Deng, A.L. Liu, X.H. Lin, X.H. Xia, W. Chen, Citrate-capped platinum nanoparticle as a smart probe for ultrasensitive mercury sensing, Anal. Chem. 86 (2014) 10955–10960.
[44] E. Schulman, W. Wu, D. Liu, Two-dimensional zeolite materials: structural and acidity properties, Materials 13 (2020) 1822.
[45] B. Gil, W.J. Roth, W. Makowski, B. Marszalek, D. Majda, Z. Olejniczak, P. Michorczyk, Facile evaluation of the crystallization and quality of the transient layered zeolite MCM-56 by infrared spectroscopy, Catal. Today 243 (2015) 39–45.
[46] B. Gil, K. Kalahurska, A. Kowalczyk, A study of the external and internal sites of 2D and 3D zeolites through the FTIR investigation of the adsorption of ammonia and pivalonitrile, Appl. Catal. A: Gen. 578 (2019) 63–69.
[47] M. Thommes, K. Kaneko, A.V. Neimark, J.P. Olivier, F. Rodriguez-Reinoso, J. Rouquerol, K.S.W. Sing, Physisorption of gases, with special reference to the evaluation of surface area and pore size distribution (IUPAC technical report), Pure Appl. Chem. 87 (2015) 1051–1069.
[48] C.A. Schneider, W.S. Rasband, K.W. Eliceiri, NIH image to ImageJ: 25 years of image analysis, Nat. Methods 9 (2012) 671–675.
[49] W.J. Roth, B. Gil, W. Makowski, B. Marszalek, P. Eliasova, Layer like porous materials with hierarchical structure, Chem. Soc. Rev. 45 (2016) 3400–3438.
[50] W.J. Roth, D.L. Dorset, G.J. Kennedy, Discovery of new MWW family zeolite EMM-10: identification of EMM-10P as the missing MWW precursor with disordered layers, Microporous Mesoporous Mater. 142 (2011) 168–177.
[51] W.J. Roth, J. Čejka, R. Millini, E. Montanari, B. Gil, M. Kubu, Swelling and interlayer chemistry of layered MWW zeolites MCM-22 and MCM-56 with high Al content, Chem. Mater. 27 (2015) 4620–4629.
[52] K. Kalahurska, P.P. Ziemianski, W.J. Roth, B. Gil, From colloidal dispersions of zeolite monolayers to effective solid catalysts in transformations of bulky organic molecules: role of freeze-drying and dialysis, Molecules 26 (2021), 2076.
[53] G.G. Juttu, R.F. Lobo, Characterization and catalytic properties of MCM-56 and MCM-22 zeolites, Microporous Mesoporous Mater. 40 (2000) 9–23.
[54] J.L. Schlenker, B.K. Peterson, Computed X-ray powder diffraction patterns for ultrasmall zeolite crystals, J. Appl. Crystallogr. 29 (1996) 178–185.